Ocean Sci. Discuss., 7, 477–500, 2010
www.ocean-sci-discuss.net/7/477/2010/
© Author(s) 2010. This work is distributed under
the Creative Commons Attribution 3.0 License.

Ocean Science Discussions

This discussion paper is/has been under review for the journal Ocean Science (OS).
Please refer to the corresponding final paper in OS if available.

Sensitivity study of wind forcing in a numerical model of mesoscale eddies in the lee of Hawaii islands

M. Kersalé[1], A. M. Doglioli[2], and A. A. Petrenko[2]

[1]Aix-Marseille Université, OSU/Centre d'Océanologie de Marseille, Marseille, France
[2]Aix-Marseille Université; CNRS; IRD; LOPB-UMR 6535, Laboratoire d'Océanographie Physique et de Biogéochimique, OSU/Centre d'Océanologie de Marseille, Marseille, France

Received: 8 February 2010 – Accepted: 21 February 2010 – Published: 10 March 2010

Correspondence to: A. M. Doglioli (andrea.doglioli@univmed.fr)

Published by Copernicus Publications on behalf of the European Geosciences Union.

Abstract

The oceanic circulation around the Hawaiian archipelago is characterized by a complex circulation and the presence of mesoscale eddies west of the islands. These eddies typically develop and persist for weeks to several months in the area during persistent trade wind conditions. In order to find the best setup of a regional ocean model and to better understand the role of the wind forcing in the eddy formation, we compare numerical results obtained using two different wind stress databases: COADS and QuikSCAT. A detailed comparative analysis of wind forcing, modeled kinetic energy and eddy generation is proposed. Moreover, numerical cyclonic eddies are compared with the ones observed during the cruises E-FLUX (Dickey et al., 2008).

The main features of the ocean circulation in the area are well reproduced by our model forced by both COADS and QuickSCAT climatologies. Nevertheless, significant differences appear in the levels of kinetic energy and vorticity. The wind-forcing spatial resolution clearly affects the way in which the wind momentum feeds the mesoscale phenomena, and, the higher the resolution, the more realistic the ocean circulation. In particular, the simulation forced by QuikSCAT wind data reproduces well the observed energetic mesoscale structures and their hydrological characteristics and behavior.

1 Introduction

The oceanic area around the Hawaiian archipelago exhibits a complex circulation characterized by the presence of mesoscale eddies west of the islands. This circulation is mainly due to the effects of the archipelago topographic forcing on both the North Equatorial Current (NEC) and the trade wind. The blocking effect of the Hawaiian islands bathymetry on the oceanic flow is similar to the one of these islands' topography on the wind.

The NEC is a broad westward flow, constituting the southern part of the North Pacific subtropical gyre. When the NEC encounters the island of Hawaii, it is deflected towards

OSD

7, 477–500, 2010

the south, but also generates a northern branch (Lumpkin, 1998). The northern branch is known as the North Hawaiian Ridge Current (NHRC), flowing coherently along the islands at an average speed of 0.10–0.15 m s^{-1} (Qiu et al., 1997). The wake generated by the Hawaiian island is thought responsible for the formation of the Hawaiian Lee Counter Current (HLCC). By a classical mechanism of formation of eddies in the lee of an obstacle, the wake can also generate the mesoscale eddies, which are observed west of the archipelago (Aristegui et al., 1994, 1997; Barton et al., 2000). South (North) of the HLCC these eddies are typically anticyclonic (cyclonic).

A second mechanism could also explain the formation of the Hawaiian mesoscale eddies. As explained by Smith and Grubisic (1993), the Hawaiian archipelago presents a series of high vertical obstacles to the wind. The islands act as barriers to the trade winds, which are confined below the tropopause and constrained to flow around the topography (Chavanne et al., 2002). The wind stress variations in the lee of the Hawaiian Islands drive divergent and convergent Ekman transports in the upper layer of the ocean. And, in particular, the acceleration of the persistent northeasterly trade winds through the Alenuihaha Channel separating these islands is the second mechanism generating mesoscale eddies (Patzert, 1969). This mechanism can create cyclonic eddies south of the HLCC, in the region where the previous mechanism was favoring anticyclonic eddies.

Historical hydrographic and satellite data sets (Patzert, 1969; Lumpkin, 1998; Chavanne et al., 2002; Seki et al., 2001, 2002; Bidigare et al., 2003) indicate that mesoscale eddies typically develop and persist for weeks to several months west of the Hawaiian archipelago during persistent trade wind conditions. Moreover, interdisciplinary observations of mesoscale eddies were recently made west of the Big Island of Hawaii combining different data from ships, surface drifters and satellite sensors (Dickey et al., 2008, project E-FLUX). During the cruises E-Flux I and III, two cold-core cyclonic mesoscale eddies, *Noah* and *Opal*, respectively, have been found.

To simulate the oceanic circulation around the Hawaiian islands, we used a version of the model ROMS (Regional Oceanic Modeling System) provided with the following

ROMSTOOLS (http://roms.mpl.ird.fr). This modeling system is increasingly used, since its functionality and robustness have been demonstrated. Different databases can be used to provide atmospheric forcing to ROMS model, such as COADS (Comprehensive Ocean-Atmosphere Data Set Project) and data collected by NASA's SeaWinds Scatterometer aboard QuikSCAT. Monthly mean values from COADS was compared to monthly mean wind speed and direction from Canadian weather buoys in the northeast Pacific (Cherniawsky and Crawford, 1996). Wind speed measurements from QuikSCAT scatterometer were validated by comparison with independent data. For instance, they were compared with meteorological analyses (Renfrew et al., 2009) over the Denmark Strait, or with wind speeds computed from RADARSAT-1 synthetic aperture radar (SAR) in the Gulf of Alaska (Monaldo et al., 2004). Concerning ocean modeling, the influence of COADS versus QuikSCAT wind data on oceanic circulation was analysed in the California Current System (Penven et al., 2002). On the North equatorial central Pacific, an ocean model forced by COADS wind versus one forced by the NCEP-NCAR (National Centers for Environmental Prediction - National Center for Atmospheric Research) reanalysis wind were used to compare the observations of ocean heat content (Wu and Xie, 2003). Independent observations of oceanic circulation was investigated with an ocean model forced by QuikSCAT wind data in different regions: Hawaiian Islands (Xie et al., 2001) and Southern Benguela coastal upwelling system (Blanke et al., 2005).

The main purpose of this study is to compare the oceanic circulation around Hawaii simulated with both COADS and QuikSCAT wind data, with particular attention to wind-driven mesoscale eddy generation. A similar work has been done recently (Calil et al., 2008) but was not known to us at the beginning of our work. The fact that the model setup is very similar to ours confirms our numerical methodology. Similarities and differences will be treated in the discussion section.

The paper is organized as follows: Sect. 2 introduces briefly the numerical model, the main simulation and eddy tracking parameters before discussing the variability in the surface wind stress in both situations. Section 3 presents the model sensitivity. This

part will allow us to analyze whether the model reproduces the generation of mesoscale eddies to the west of the Hawaiian archipelago. In Sect. 4, we analyse which simulation is the more realistic. Our conclusions are drawn in Sect. 6.

2 Materials and methods

2.1 Ocean model

Our circulation model is based on the IRD (Institut de Recherche pour le Développement) version of the Regional Ocean Modeling System (ROMS). The reader is referred to Shchepetkin and McWilliams (2003, 2005) for a more complete description of the numerical code. The model domain extends from 154° W to 161° W and from 18° N to 23° N (Fig. 1).

Its grid, forcing, initial and boundary conditions were built with the ROMSTOOLS package (Penven, 2003). The model grid is 69 × 53 points with a resolution of $\frac{1}{10}^{\circ}$ corresponding to about 10 km in mean grid spacing, which allows a correct sampling of the first baroclinic Rossby radius of deformation throughout the whole area (about 60 km according to Chelton et al., 1998). The horizontal grid is isotropic with no introduction of asymmetry in the horizontal dissipation of turbulence. It therefore provides a fair representation of mesoscale dynamics. The model has 32 vertical levels, and the vertical s-coordinate is stretched for boundary layer resolution. The bottom topography is derived from a $2'$ resolution database (Smith and Sandwell, 1997). Although a numerical scheme associated with a specific equation of state limits errors in the computation of the horizontal pressure gradient (Shchepetkin and McWilliams, 2003), the bathymetry field, h, must be filtered to keep the slope parameter, r, as $r = \frac{|\nabla h|}{2h} \leq 0.25$ (Beckmann and Haidvogel, 1993). Respecting the CFL criterion, the external (internal) timestep has been fixed equal to 12 s (720 s).

At the four lateral boundaries facing the open ocean, the model solution is connected to the surroundings by an active, implicit and upstream-biased radiation condition

OSD
7, 477–500, 2010

(Marchesiello et al., 2001). Under inflow conditions, the solution at the boundary is nudged toward temperature-, salinity- and geostrophic velocity-fields calculated from Levitus 1998 climatology (NODCWOA98 data provided by the NOAA/OAR/ESRL PSD, Boulder, Colorado, USA, from their Web site at http://www.cdc.noaa.gov/), which is also used for the initial state of the model. The geostrophic velocity is referenced to the 2000 m level. The width of the nudging border is 100 km, and the maximum viscosity value for the sponge layer is set to 800 $m^2 s^{-1}$.

At the surface, the heat and fresh water fluxes introduced in the model are extracted from the Comprehensive Ocean-Atmosphere Data Set (COADS, Da Silva et al., 1994). As regards wind stress, two different database are used in this work. Firstly, we used a monthly mean climatology computed from COADS dataset (1945–1989) giving data with spatial resolution of $\frac{1}{2}^\circ$ (hereinafter C-run). Secondly, we used a monthly mean climatology computed from satellite-based QuikSCAT dataset (2000–2007, Callahan and Lungu, 2006) gridded at $\frac{1}{4}^\circ$ resolution (hereinafter Q-run).

In both cases, we run 10-year simulations with model outputs averaged and stored every 3 days of simulation.

2.2 Eddy tracking and characterization

In this paper we focus particularly on the tenth year of simulation, ensuring a good stability of the model. To detect eddies, we selected a threshold value of the sea surface height (ssh) of |5| cm. We choose to set this value to one third of the typical ssh anomaly generated by anticyclonic eddies in the Hawaii region (i.e. 15 cm, according to Firing and Merrifield, 2004). Each cyclone (anticyclone) is then listed by the letter *C* (*A*) followed by the number corresponding to their temporal appearance. To indicate if eddies are observed in the C-run (Q-run), the letter designating them is in capital (lowercase) letters. In the following we focus particularly on *C5* (C-run) and *c1* (Q-run), that both last seven months in the tenth year of the two simulations. *C5* (*c1*) appears in April (January) and disappears in October (July). Both numerical cyclones are chosen because they are spatially and temporally representative of cyclone *Opal* studied

CC BY

during the cruise E-FLUX III (10–28 March, 2005) and observed on SST satellite images from February to April of that year (Nencioli et al., 2008). The numerical eddies resembles the most *Opal* on 14 April for *C5* and 29 March for *c1*.

Following Dickey et al. (2008), we define the radial extent of the eddy as the distance between the locations where isopycnal and isotherm surfaces became nearly horizontal. Indeed, according to these authors, the $\sigma - t_{24}$ (i.e. $\sigma - t = 24\,\mathrm{kg\,m^{-3}}$) isopycnal surface proved to be an important reference in determining the general characteristics of cyclones in this area. Moreover, we calculated the East-West (North-South) components of the horizontal velocity vector along a North-South (East-West) transect for each numerical eddy. In this way we can both (i) estimate the position of the eddy center, as the location where the components of the horizontal velocity are very small and (ii) calculate the eddy radius, as the maximum distance until which, starting at the center, the intensity of the velocity increases linearly (i.e. solid body rotation, e.g. Nencioli et al., 2008). This latter distance allows us to also check the previous evaluation of the eddy extent.

2.3 Wind forcing comparison

As foreseen, the monthly averaged values of the two wind stress datasets have significant differences. The difference between the QuikSCAT and COADS values calculated at each grid point shows interesting spatial patterns (Fig. 2). Far from the archipelago, the difference is small during the whole year. Instead, near the islands, the QuikSCAT values are generally stronger than the COADS ones. From April to September, strong differences are observed southwest of the Alenuihaha Channel and south of the Big Island. In particular, the difference reaches values up to $+0.1\,\mathrm{Nm^{-2}}$ southwest of the Alenuihaha Channel.

To summarize the occurrence of winds in this area, we plot wind roses for each database at the point (20° N, 156° W). Figure 3 shows that an unidirectional wind regime, stemming from the north-east (i.e. trade wind), is predominant in both datasets. In COADS, approximately 15% of the time the wind comes from the east and 85% from

OSD
7, 477–500, 2010

the north-east (Fig. 3a); while, in QuikSCAT, the wind always corresponds to the north-easterly trade winds (Fig. 3b). Moreover, in COADS, the prevailing wind stress intensity is in the range 0.06–0.08 Nm^{-2}; while, in QuikSCAT, the values are much more intense and the prevailing range is 0.10–0.12 Nm^{-2}.

3 Results

In general, our model, both in Q-run and C-run, reproduces well the ocean circulation of the study area described in Sect. 1: the NEC split in two branches when it encounters the Hawaii Archipelago. In the wake of the islands the HLCC and the mesoscale eddies form. For a more detailed comparison between the two runs, in the following section, we analyze the kinetic energy, the eddies' generation and spread and the cyclones' characteristics.

3.1 Kinetic energy

The temporal evolutions of the volume-averaged and surface-averaged kinetic energies for both simulations are reported in Fig. 4.

The Q-run results are generally more energetic than the C-run ones. Indeed, the 10-year mean value of volume-(surface-) averaged kinetic energy for the C-run is 26 (200) $cm^2\,s^{-2}$, while being 30 (400) $cm^2\,s^{-2}$ for the Q-run. Moreover, the kinetic energy has a lower temporal variability in the C-run than in the Q-run.

In order to analyze the ergodicity, we calculate the total kinetic energy (TKE) at 10-m depth and then the eddy kinetic energy (EKE) in two different ways: EKE_{surf} is the difference between TKE and its surface average $<TKE> = \frac{1}{S}\int_S TKE(x,y,t)dxdy$, while EKE_{time} is the difference between TKE and its monthly time average $\overline{TKE} = \frac{1}{T}\int_0^T TKE(x,y,t)dt$. In this latter calculation, a monthly variability is considered sufficient because in the study area there is no significant seasonal variability. For the C-run, the higher values of TKE are far from the island, in meanders of the HLCC

OSD
7, 477–500, 2010

(Fig. 5a). Moreover, EKE_{surf} and EKE_{time} have very similar patterns. For the Q-run, instead, the highest values of TKE are concentrated in eddies near the islands (Fig. 5b) but again EKE_{surf} and EKE_{time} have similar patterns.

3.2 Eddies' generation and spread

In Fig. 6 we show the relative vorticity field at 10-m depth on the first day of March, April and May for both C-run and Q-run. Several eddies, both cyclonic and anticyclonic are present in the two simulations. Nevertheless, structures from the C-run are less intense and defined than the ones from the Q-run. The cyclonic minimum value of relative vorticity is equal to $-2.46\ 10^{-5}$ $[s]^{-1}$ in May for the C-run and to $-3{,}48\ 10^{-5}$ $[s]^{-1}$ in March for the Q-run. The anticyclonic maximum value of relative vorticity is equal to $+2{,}36\ 10^{-5}$ $[s]^{-1}$ in May for the C-run and to $+3{,}96\ 10^{-5}$ $[s]^{-1}$ in May for the Q-run. Moreover, the anticyclonic relative vorticity values are generally twice higher for Q-run than C-run. Two sites of wind genesis of cyclonic eddies are observed: the channel between the Kauai and Oahu islands and the Alenuihaha Channel. In the first location *C4*, *C6* (C-run) and *c2* (Q-run) form, while in the second one *C5* (C-run) and *c1* (Q-run). The northern location (Kauai-Oahu) is located on the cyclonic edge of the HLCC, while the southern location (Alenuihaha) on the anticyclonic one. Then it is not surprising that, in the latter site, wind-generated cyclones are associated with anticyclones.

After their formation, the eddies generally move westward. In general, we observed that the cyclones move toward the north-west and anticyclones to the south-west. This fact has been explained by Cushman-Roisin (1994) in terms of potential vorticity conservation on a β-plane and then observed in satellite data by Morrow et al. (2004). Nevertheless, in the Alenuihaha Channel, the funneling of the wind can push the cyclones to the south (April to May for *C5* Fig. 6a) or to the south-east (March to April for *c1* Fig. 6b). This movement is then blocked by the Big Island, where the topographical friction generates additional anticyclonic vorticity. That process is well observed in the Q-run results, where the anticyclones are better defined than in the C-run.

OSD
7, 477–500, 2010

The presence of the eddies in the model domain ranges from 2 to 7 months, without notable differences neither between anticyclones and cyclones, nor between C-run and Q-run.

3.3 Cyclones' characteristics

Depth profiles of temperature with $\sigma - t_{23.6}$, $\sigma - t_{23.8}$, $\sigma - t_{24}$ isopycnals are shown in Fig. 7.

The sections reveal an intense doming of isothermal and isopycnal surfaces with outcropping at the surface. Following the method used by Dickey et al. (2008), we obtain an estimate of the diameter of *C5* (*c1*) of about 180 (220) km.

We report zonal and meridional components of the 40-m depth horizontal velocity along meridional and zonal transect, respectively, for eddies *C5* and *c1* in Fig. 8. We choose this depth for a direct comparison with in situ measurement performed by Nencioli et al. (2008) inside the cyclone *Opal*. The position of an eddy's center can be located at the point of minimal velocity, i.e. in this case near 19.5° N, 156.6° W for both eddies.

In Fig. 9 we show the distribution of the zonal and meridional component of the 40-m depth horizontal velocity with respect to the distance from the eddy center for both *C5* (C-run, 14 April) and *c1* (Q-run, 29 March). Both eddies are characterized by values that increase linearly with distance from the center until peaking and then slowly decaying. For *C5*, the peak value is about 0.35 m s^{-1}, while it nearly reaches 0.60 m s^{-1} for *c1*. The linear part corresponds to the solid-body rotation core of the eddy. Otherwise, both eddies appear quite asymmetric and stretched. Hence it is difficult to define with precision an eddy radius. Nonetheless, it appears clearly that the part in solid body rotation has a diameter smaller than the one estimated above on the basis of the isopycnal outcropping.

OSD
7, 477–500, 2010

4 Discussion

The ocean circulation generated by the model forced by both COADS and QuickSCAT climatologies comply with the pattern of the regional oceanic circulation by Lumpkin (1998), but significant differences appears between the C-run and the Q-run. A higher temporal variability of the kinetic energy appears clearly in the Q-run with respect to the C-run. Since both simulations seem to satisfy the ergodic hypothesis, we think that this temporal variability is induced by the higher spatial variability of the QuickSCAT wind forcing. Indeed, the similarity between EKE and TKE, in both C-run and Q-run, indicates that most of the wind forcing momentum feed the mesoscale phenomena and that the high values of TKE in the lee of the islands is locally generated. In agreement with Calil et al. (2008), our model results show that having good spatial resolution surface momentum forcing is vital to produce realistic levels of kinetic energy and vorticity in the ocean circulation. The COADS data resolution do not provide sufficient information to well reproduce both mechanisms that are thought to be responsible for the presence of mesoscale eddies adjacent to islands. Indeed, the C-run seems to simulate better the eddies due to instabilities associated with current flow past the islands than the ones due to the funneling of the wind between the islands. With respect the $\frac{1}{4}^{\circ}$ QuickSCAT climatology, the $\frac{1}{2}^{\circ}$ COADS one does not produce the wind acceleration through the Alenuihaha Channel and other passages between islands. Then, the eddies from the C-run are less intense and defined than the ones from the Q-run.

The detailed comparison between cold-core eddies has been performed to validate the model with respect to the observations of the eddy *Opal* (Dickey et al., 2008). In the same area, period and conditions of the E- Flux III field campaigns, i.e. in March and April, downwind of the Alenuihaha Channel and during strong, persistent northeasterly trade winds, our model generates cyclonic eddies in both C-run and Q-run. Moreover, the model reproduces well the intense doming of isothermal and isopycnal associated with the cyclonic structures. Nevertheless, the C-run cyclones appear smaller in diameter and less energetic than the Q-run ones and *Opal*. Moreover the maximum

OSD
7, 477–500, 2010

velocity in the Q-run cyclones are higher than the C-run ones and closer in amplitude to the maximum velocities measured in *Opal* (Nencioli et al., 2008). Permanence in the model domain of the cyclonic eddy is similar to that observed, but the southward drift of *Opal* is well reproduced only by *c1*. This fact suggests that this phenomenon is also due to the funneling of the wind in the Alenuihaha Channel area.

5 Conclusions

The Hawaiian archipelago has a strong influence on both the atmospheric and the oceanic circulations. In order to well reproduce the oceanic circulation in the area, it is then necessary to have, not only a high spatial resolution of the circulation model, but also a wind stress forcing data that reproduces the complexity of the atmospheric flow between the islands. In this study, we compare the oceanic circulations around Hawaii forced by COADS and QuikSCAT wind data. We obtain significant differences between the simulations using specific databases. In agreement with previous numerical studies such as the one performed by Calil et al. (2008) in the same area, but also as other ones done in different areas (e.g. Penven et al., 2002), our results suggest that higher spatial variability allows to reproduce more realistic circulation. In particular, the simulation forced by QuikSCAT wind data reproduces well the energetic mesoscale structures observed during the E-Flux field experiments (Dickey et al., 2008), including their hydrological characteristics and behavior. This setup will allow future studies that are needed to better understand the role of temporal variability and bottom friction on the behavior of mesoscale eddies and the role of these structures in the distribution of biogeochemical properties.

Acknowledgements. M. Kersalé, Master student in physical oceanography at the "Centre d'Océanologie de Marseille (COM)", thanks the "Service Informatique du COM (SIC)" for their assistance in the students' computer room. This work is in the framework of the LATEX project (http://www.com.univ-mrs.fr/LOPB/LATEX), founded by CNRS LEFE/IDAO-CYBER and Région PACA.

References

Aristegui, J., Sangra, P., Henandez-Leon, S., Canton, M., and Hernandez-Guerra, A.: Island-induced eddies in the Canary Islands, Deep-Sea Res. Pt. I, 41, 1509–1525, 1994. 479

Aristegui, J., Tett, P., Hernandez-Guerra, A., Basterretxea, G., Montero, M. F., Wild, K., Sangra, P., Hernandez-Leon, S., Canton, M., Garcia-Braun, J. A., Pacheco, M., and Barton, E. D.: The influence of island-generated eddies on chlorophyll distribution: a study of mesoscale variation around Gran Canaria, Deep-Sea Res. Pt. I, 44, 71–96, 1997. 479

Barton, E., Basterretxea, G., Flament, P., Mitchelson-Jacob, E., Jones, B., Aristegui, J., and Herrera, F.: Lee region of Gran Canaria, J. Geophys. Res., 105, 17173–17193, 2000. 479

Beckmann, A. and Haidvogel, D.: Numerical simulation of flow around a tall isolated seamount. Part 1: Problem formulation and model accuracy, J. Phys. Oceanogr., 23(8), 1736–1753, 1993. 481

Bidigare, R. R., Benitez-Nelson, C., Leonard, C. L., Quay, P. D., Parsons, M. L., Foley, D. G., and Seki, M. P.: Influence of a cyclonic eddy on microheterotroph biomass and carbon export in the lee of Hawaii, Geophys. Res. Lett., 30, 1318, doi:10.1029/2002GL016393, 2003. 479

Blanke, B., Speich, S., Bentamy, A., Roy, C., and Sow, B.: Modeling the structure and variability of the southern Benguela upwelling using QuikSCAT wind forcing, J. Geophys. Res., 110, C07018, doi:10.1029/2004JC002529, 2005. 480

Calil, P. H. R., Richards, K. J., Yanli, J., and Bidigare, R. R.: Eddy activity in the lee of the Hawaiian Islands, Deep-Sea Res. Pt. II, 55, 1179–1194, 2008. 480, 487, 488

Callahan, P. S. and Lungu, T.: QuikSCAT Science Data Product User's Manual (v3.0), Tech. rep., Jet Propul. Lab., Pasadena, CA, 91 pp., 2006. 482

Chavanne, C., Flament, P., Lumpkin, R., Dousset, B., and Bentamy, A.: Scatterometer observations of wind variations induced by oceanic islands: implications for wind-driven ocean circulation., Can. J. Remote Sens., 28, 466–474, 2002. 479

Chelton, D. B., deSzoeke, R. A., Schlax, M. G., El Naggar, K., and Siwertz, N.: Geographical variability of the first-baroclinic Rossby radius of deformation, J. Phys. Oceanogr., 28, 433–460, 1998. 481

Cherniawsky, J. Y. and Crawford, W. R.: Comparison between weather buoy and Comprehensive Ocean-Atmosphere Data Set wind data for the west coast of Canada, J. Geophys. Res., 101, 18377–18390, 1996. 480

Cushman-Roisin, B.: Introduction to Geophysical Fluid Dynamics, Prentice Hall, 1994. 485

Da Silva, A. M., Young, C. C., and Levitus, S.: Atlas of surface marine data 1994, vol. 1, algorithms and procedures, Tech. rep., U. S. Department of Commerce, NOAA, 1994. 482
Dickey, T. D., Nencioli, F., Kuwahara, V. S., Leonard, C., Black, W., Rii, Y. M., Bidigare, R. R., and Zhang, Q.: Physical and bio-optical observations of oceanic cyclones west of the island of Hawaií, Deep-Sea Res. Pt. II, 55, 1195–1217, 2008. 478, 479, 483, 486, 487, 488
Firing, Y. L. and Merrifield, M. A.: Extreme sea level events at Hawaii : Influence of mesoscale eddies, Geophys. Res. Lett., 31, L24306, doi:10.1029/2004GL021539, 2004. 482
Lumpkin, C. F.: Eddies and currents in the Hawaii islands, Ph.D. thesis, University of Hawaii, 1998. 479, 487
Marchesiello, P., McWilliams, J. C., and Shchepetkin, A.: Open boundary condition for long-term integration of regional oceanic models, Ocean Model., 3, 1–21, doi:10.1016/S1463-5003(00)00013-5, 2001. 482
Monaldo, F. M., Thompson, D. R., Pichel, W. G., and Clemente-Colon, P.: A systematic comparison of QuikSCAT and SAR ocean surface wind speeds, IEEE T. Geosci. Remote, 42, 283–291, 2004. 480
Morrow, R., Birol, F., Griffin, D., and Sudre, J.: Divergent pathways of cyclonic and anti-cyclonic ocean eddies, Geophys. Res. Lett., 31, L24311, doi:10.1029/2004GL020974, 2004. 485
Nencioli, F., Kuwahara, V. S., Dickey, T. D., Rii, Y. M., and Bidigare, R. R.: Physical dynamics and biological implications of a mesoscale eddy in the lee of Hawai'i: Cyclone Opal observations during E-FLUX III, Deep-Sea Res. Pt. II, 55, 1252–1274, 2008. 483, 486, 488
Patzert, W. C.: Eddies in Hawaiian Islands, Tech. rep., Hawaii Institute og Geophysics, University of Hawaii, 1969. 479
Penven, P.: ROMSTOOLS user guide, Tech. rep., Inst. de Rech. pour le Dév., Paris, France, http://roms.mpl.ird.fr, 2003. 481
Penven, P., McWilliams, J. C., Marchesiello, P., and Chao, Y.: Coastal Upwelling response to atmospheric wind forcing along the Pacific coast of the United States, Ocean Sciences Meeting, Honolulu, Hawaii (USA), 2002. 480, 488
Qiu, B., Koh, D. A., Lumpkin, C., and Flament, P.: Existence and formation mechanism of the North Hawaiian Ridge Current, J. Phys. Oceanogr., 27, 431–444, 1997. 479
Renfrew, I. A., Petersen, G. N., Sproson, D. A. J., Moore, G. W. K., Adiwidjaja, H., Zhang, S., and North, R.: A comparison of aircraft-based surface-layer observations over Denmark Strait and the Irminger Sea with meteorological analyses and QuikSCAT winds, Q. J. Roy. Meteor. Soc., 135, 2046–2066, 2009. 480

Seki, M. P., Polovina, J. J., Brainard, R. E., Bidigare, R. R., Leonard, C. L., and Foley, D. G.: Biological enhancement at cyclonic eddies tracked with GOES thermal imagery in Hawaiian waters, Geophys. Res. Lett., 28, 1583–1586, 2001. 479

Seki, M. P., Lumpkin, R., and Flament, P.: Hawaii cyclonic eddies and blue marlin catches: the case study of the 1995 Hawaiian International Billfish Tournament, J. Oceanogr., 58, 739–745, 2002. 479

Shchepetkin, A. F. and McWilliams, J. C.: A method for computing horizontal pressure-gradient force in an oceanic model with nonaligned vertical coordinate, J. Geophys. Res., 108, 3090, doi:10.1029/2001JC001047, 2003. 481

Shchepetkin, A. F. and McWilliams, J. C.: The regional oceanic modeling system (ROMS): a split-explicit, free-surface, topography-following-coordinate oceanic model, Ocean Model., 9, 347–304, doi:10.1016/j.ocemod.2004.08.002, 2005. 481

Smith, R. B. and Grubisic, V.: Aerial observations of Hawaii's wake, J. Atmos. Sci., 50, 3728–3750, 1993. 479

Smith, W. H. F. and Sandwell, D. T.: Global sea floor topography from satellite altimetry and ship depth soundings, Science, 227, 1956–1962, doi:10.1126/science.277.5334.1956, 1997. 481

Wu, R. and Xie, S.: On Equatorial Pacific surface wind changes around 1977: NCEP-NCAR reanalysis versus COADS observations , J. Climate, 16, 167–173, 2003. 480

Xie, S., Liu, W., Liu, Q., and Nonaka, M.: Far-Reaching Effects of the Hawaiian Islands on the Pacific Ocean-Atmosphere System, Science, 292, 2057–2060, 2001. 480

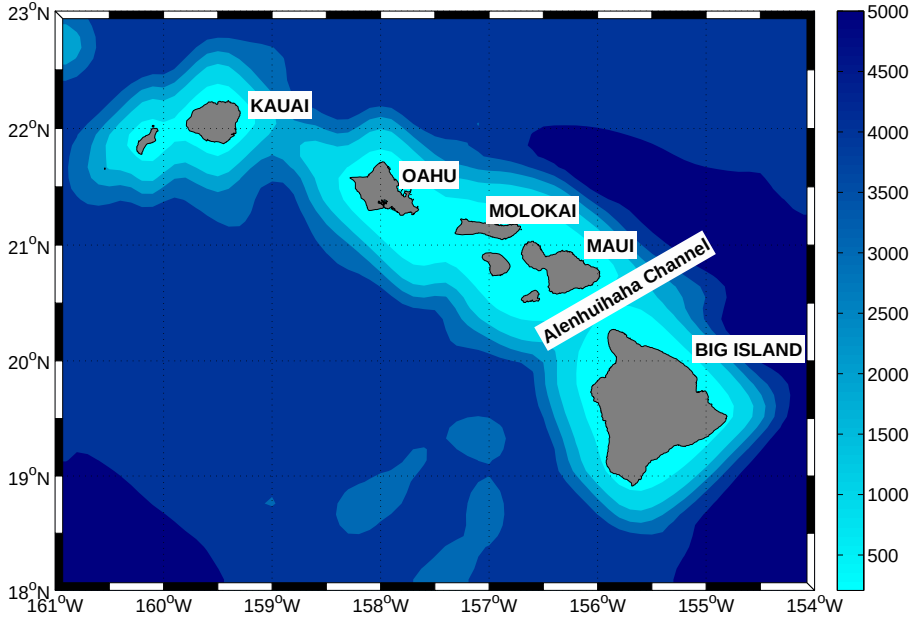

Fig. 1. Model domain and bathymetry [m]. Islands' names and coastline at higher resolution are reported for geographical information.

OSD

7, 477–500, 2010

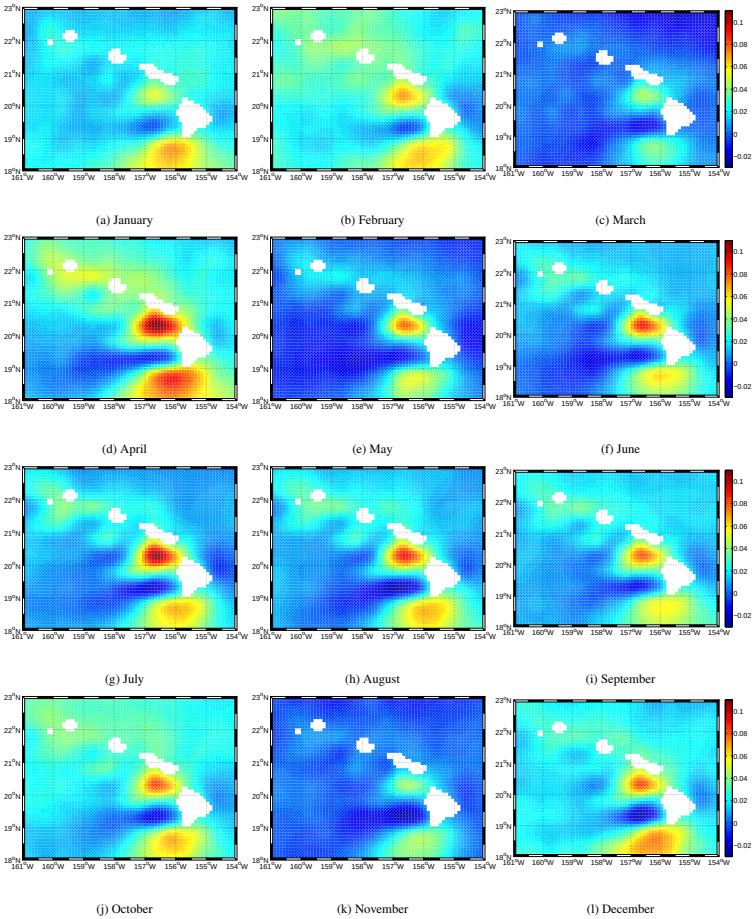

Fig. 2. Difference between QuikSCAT and COADS monthly-averaged wind stress values [Nm^{-2}].

OSD
7, 477–500, 2010

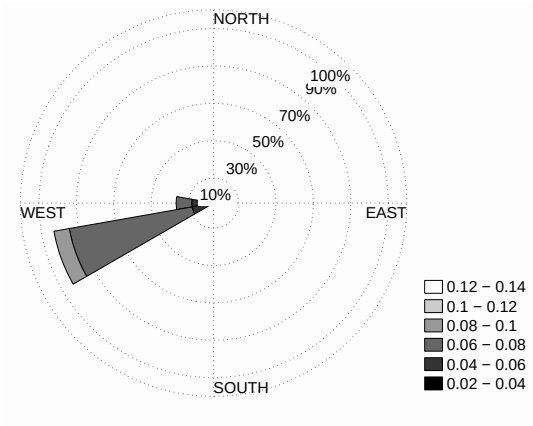

(a) COADS

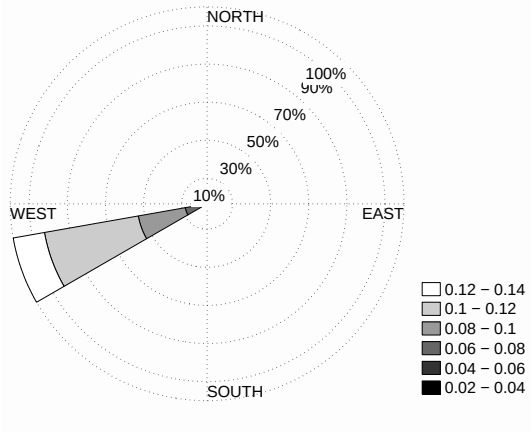

(b) QuikSCAT

Fig. 3. Wind rose showing the relative frequency of direction and intensity [Nm^{-2}] of the wind stress outside the Alenuihaha Channel (20° N, 156° W) from COADS (left) and QuikSCAT (right) climatologies.

OSD
7, 477–500, 2010

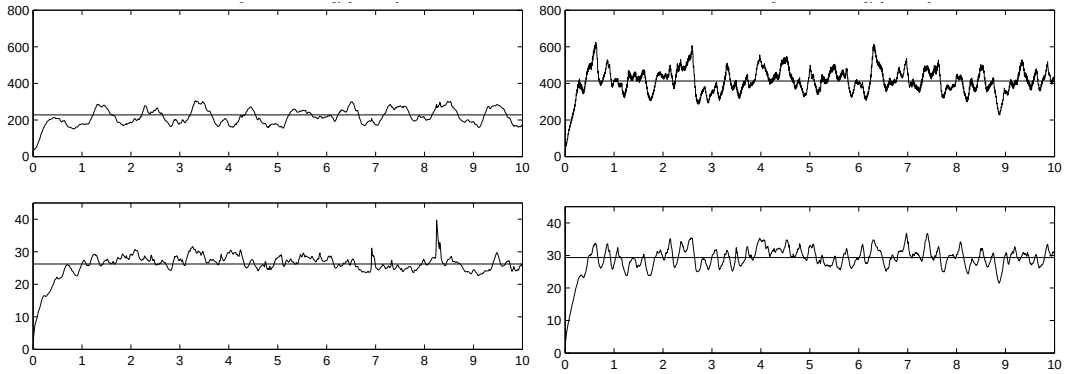

(a) C-run (b) Q-run

Fig. 4. Temporal evolution [model time, years] of surface-averaged (top) and volume-averaged (bottom) kinetic energy [$cm^2 s^{-2}$] for C-run (left) and Q-run (right). The horizontal line indicates the 10-year mean value.

OSD

7, 477–500, 2010

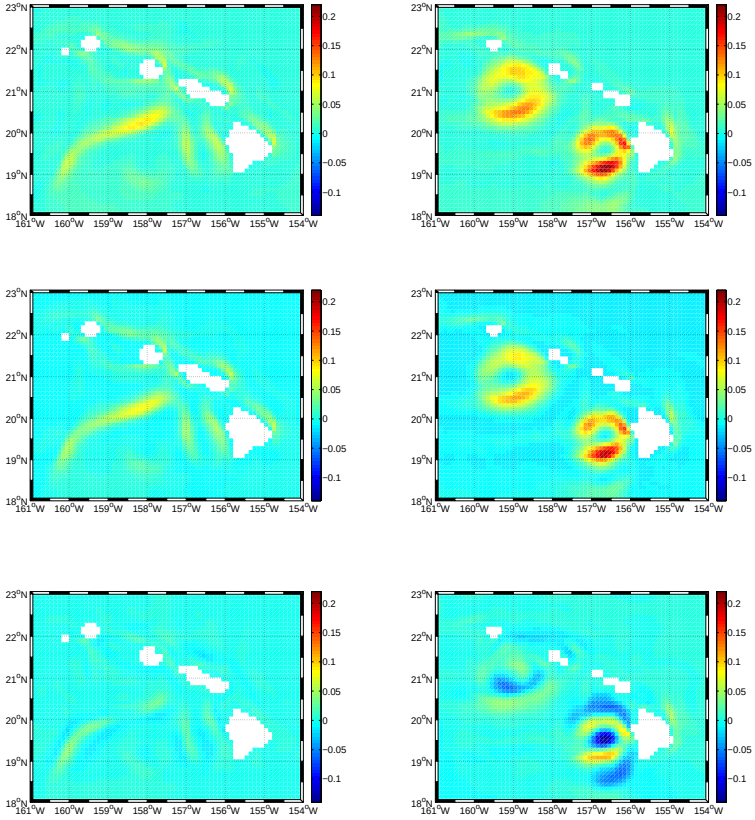

(a) C-run (b) Q-run

Fig. 5. TKE (top), EKE_{surf} (medium) and EKE_{time} (bottom) [$cm^2\ s^{-2}$] at 10-m depth for the C-run (left) and the Q-run (right). TKE and EKE_{surf} are calculated on 14 April for the C-run and on 29 March for the Q-run.

OSD
7, 477–500, 2010

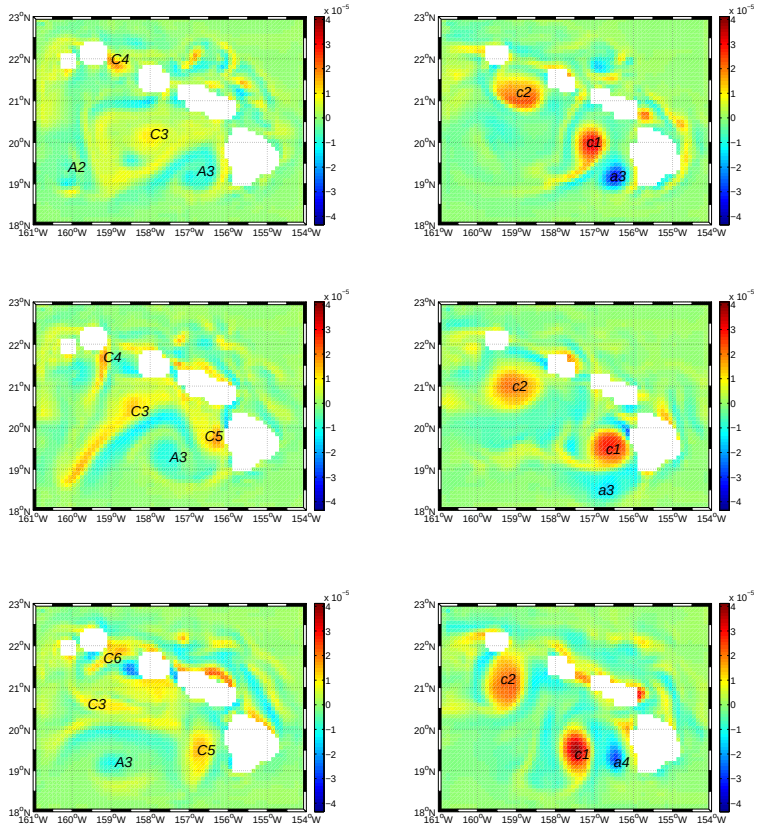

(a) C-run (b) Q-run

Fig. 6. Relative vorticity field at 10-m depth on the first day of March (top), April (medium) and May (bottom), for the C-run (left) and the Q-run (right). Eddy identification is also reported, see the text for explanation.

OSD
7, 477–500, 2010




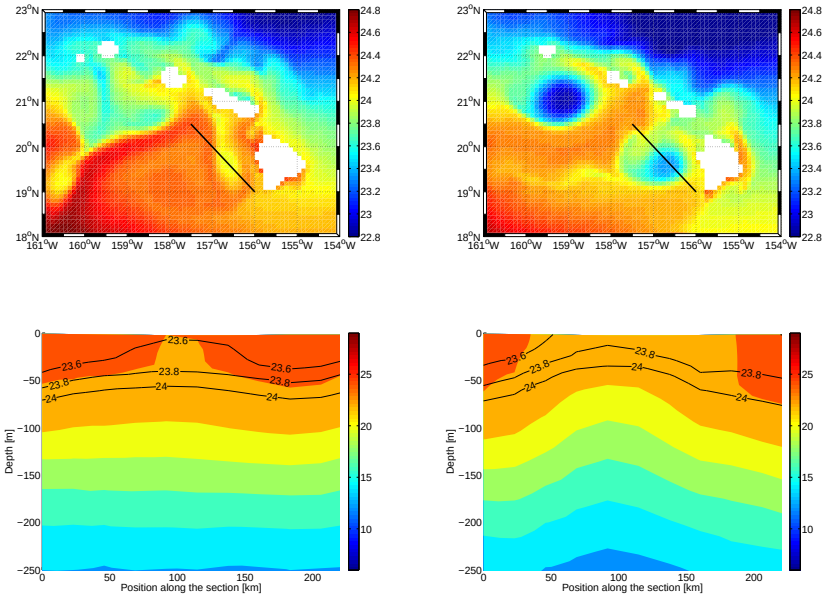

(a) C-run (b) Q-run

Fig. 7. Surface temperature maps (top) with position of the transects (black straight line) crossing the center of the eddy *C5* (left) and *c1* (right) and vertical sections (bottom) of temperature on 14 April for the C-run (left) and on 29 March for the Q-run (right). The black lines in the vertical sections represent $\sigma - t_{23.6}$, $\sigma - t_{23.8}$ and $\sigma - t_{24}$ isopycnals.

OSD
7, 477–500, 2010

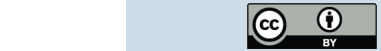

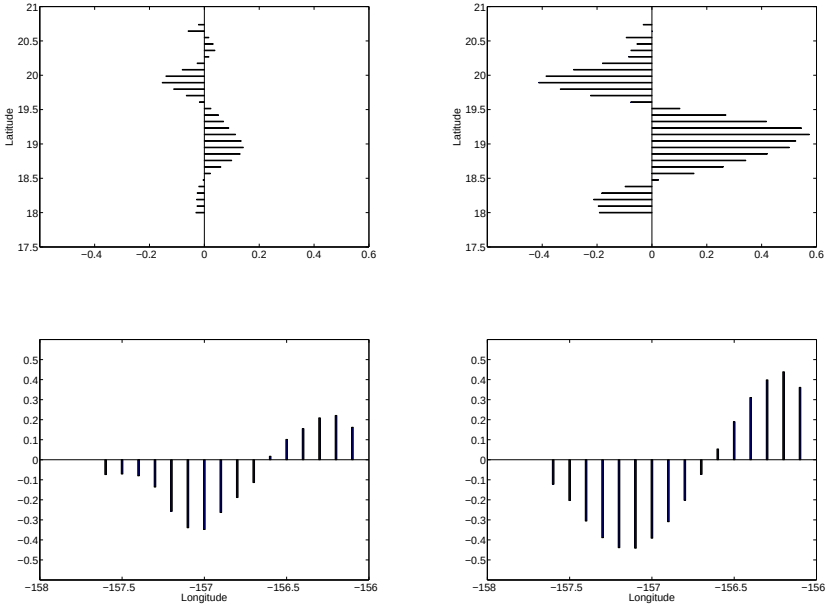

(a) C-run

(b) Q-run

Fig. 8. East-West component of the 40-m depth horizontal velocity [m s^{-1}] vector along a North-South transect (top) and North-South component along a East-West transect of the eddy *C5* (C-run, 14 April, left) and of the eddy *c1* (Q-run, 29 March, right).

OSD

7, 477–500, 2010

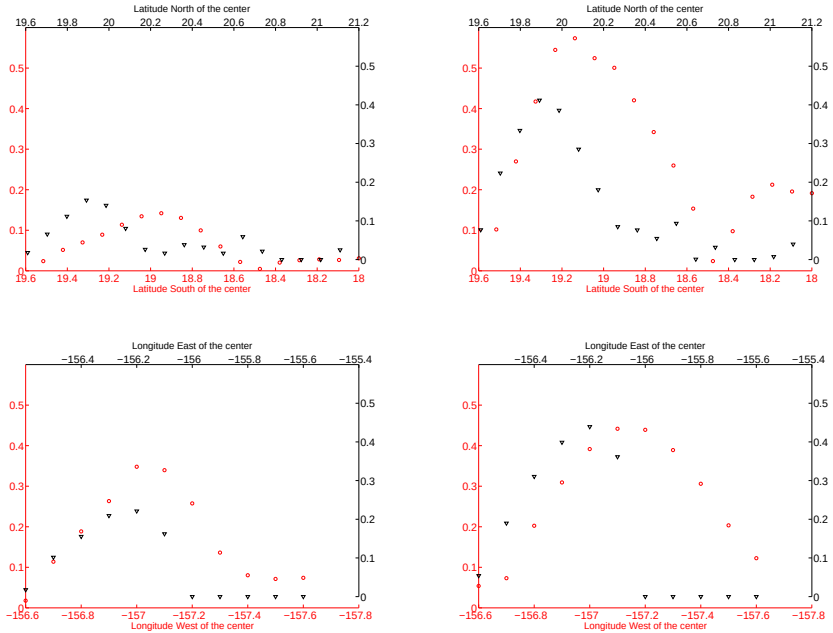

(a) C-run

(b) Q-run

Fig. 9. Distribution of zonal (top) and meridional (bottom) components of the 40-m depth horizontal velocity [m s^{-1}] with respect to the center of the eddy *C5* (C-run, 14 April, left) and of the eddy *c1* (Q-run, 29 March, right).

OSD

7, 477–500, 2010